# Experimental and Theoretical Study of the Adsorption of a Diblock Copolymer to Interfaces between Two Homopolymers

**Benedict J. Reynolds,[†] Megan L. Ruegg,[†] Thomas E. Mates,[‡] C. J. Radke,*[,†,§] and Nitash P. Balsara*[,†,⊥]**

*Department of Chemical Engineering, University of California, Berkeley, California 94720; Materials Department, University of California, Santa Barbara, California 93106; Earth Science Division, Lawrence Berkeley National Laboratory, University of California, Berkeley, California 94720; and Materials Sciences Division, and Environmental Energy Technologies Division, Lawrence Berkeley National Laboratory, University of California, Berkeley, California 94720*

*Received November 29, 2004; Revised Manuscript Received February 16, 2005*

ABSTRACT: Dynamic secondary-ion mass spectrometry (SIMS) was used to measure equilibrium volume-fraction profiles of a symmetric diblock copolymer at a polymer/polymer interface. The three polymers were a saturated polybutadiene with 90% 1,2-addition (sPB90) homopolymer, a saturated polybutadiene with 63% 1,2-addition (sPB63) homopolymer, and a sPB90−sPB63 diblock copolymer. The molecular weights of the homopolymers were chosen such that the sPB90/sPB63 blend was deep in the two-phase region. The experimentally determined volume-fraction profiles were compared with self-consistent-field theory calculations (SCFT). The statistical segment lengths and the Flory−Huggins interaction parameter were obtained independently from small-angle neutron scattering (SANS) measurements on a low molecular weight, homogeneous binary sPB90/sPB63 blend. Thus, no adjustable parameters were used in the SCFT calculations. Adsorption isotherms and the measured diblock copolymer volume-fraction profiles are in excellent agreement with the SCFT calculations. This work demonstrates that Flory−Huggins interaction parameters and statistical segment lengths determined by SANS can be used to predict complex phase behavior, including interfacial adsorption of block copolymers.

## Introduction

Blending polymers is an effective means to create new materials with properties that cannot be achieved with a single polymer. Because most polymers are strongly immiscible in one another, the resultant blends are emulsions, and like all emulsions additives are required to stabilize them. The emulsification of immiscible polymers using diblock copolymers has been extensively studied. Diblock copolymers are known to adsorb at the interface between homopolymers, thereby reducing the interfacial tension, stabilizing the emulsion, and improving the interfacial adhesion.[1−9] Both the processing history and the properties of the interface are important in determining the resultant emulsion behavior.

For some polymer blends, the interfacial tension can be reduced to such an extent by the addition of suitable block copolymers that the emulsion becomes thermodynamically stable. These systems are termed microemulsions. Because microemulsions represent an equilibrium state, their behavior is independent of processing history. The morphologies of microemulsions have been extensively studied for blends of two homopolymers (A and B) and a diblock copolymer (A−B).[10−19] The promise of morphological control over the resultant emulsion drives further study into the thermodynamics of these ternary blends. A characteristic of emulsions is that their behavior can be described in terms of interacting interfaces; thus, an important first step in understanding emulsions is to understand the interfaces. Considering the large research effort into the morphology of A/B/A−B ternary blends, (see refs 10-19 for representative examples), the behavior of the interface itself has received comparatively less attention.[20−39]

Properties of polymer/polymer interfaces, such as the interfacial tension[20−23] and the amount of adsorbed diblock copolymer,[24−27,37,39] are amenable to experimental measurement. Forward recoil spectrometry (FRES), neutron reflectivity,[40] and dynamic secondary-ion mass spectrometry (SIMS)[41] have been used to measure the adsorption of a diblock copolymer to a polymer/polymer interface. Neutron reflectivity and SIMS have sufficiently high resolutions (0.5 and 5 nm, respectively) that they can measure the interfacial segment density profiles. Conversely, the resolution of FRES (80 nm) means that it is only useful for determining adsorbed amounts. Numerous neutron reflectivity and SIMS measurements have qualitatively confirmed the intuitive expectation that the A block of the diblock copolymer extends into the A homopolymer phase, whereas the B block extends into the B homopolymer phase.[25,28−35] Quantitative investigations of diblock copolymers at polymer/polymer interfaces are scarce, and little work has been done investigating the amount of adsorbed diblock copolymer as a function of the copolymer concentration in the bulk (often referred to as the adsorption isotherm).[24−27,37,38]

In a rigorous set of experiments, Shull et al. and Dai et al. used both FRES and neutron reflectivity to construct adsorption isotherms for polystyrene (PS)−polyvinylpyridine (PVP) diblock copolymers at a PS/PVP interface.[25,26,37−39] The diblock copolymers studied by Shull et al. and Dai et al. were all asymmetric with much greater solubilities in the PS than in the PVP phase. The adsorption isotherms were fit quantitatively using self-consistent-field theory with the Flory−Huggins interaction parameter, $\chi$, as an adjustable param-

[†] University of California, Berkeley.
[‡] University of California, Santa Barbara.
[§] Earth Science Division, Lawrence Berkeley National Laboratory.
[⊥] Materials Sciences Division, and Environmental Energy Technologies Division, Lawrence Berkeley National Laboratory.

10.1021/ma047539s CCC: $30.25 
Published on Web 04/09/2005

eter. In fact, these experiments were the first determination of $\chi$ between PS and PVP.[37] Self-consistent-field theory using the same value of $\chi$ was also found to reproduce the volume-fraction profile of the diblock copolymer at the interface measured by neutron reflectivity.[25]

There is considerable debate in the literature about the interpretation of experimentally determined $\chi$ parameters. A body of literature suggests that $\chi$ parameters determined from a particular mixture cannot be used to predict the thermodynamic properties of other mixtures with different volume fractions, molecular weights, or polymer architectures.[42−44] The relationship between $\chi$ parameters determined by small-angle neutron scattering (SANS) from homogeneous blends and adsorption isotherms is not clear at this juncture.

Following the work of Shull et al. and Dai et al., we investigate the adsorption of a symmetric A−B diblock copolymer to a symmetric A/B polymer/polymer interface. The polymers are model polyolefins: A is 90% 1,2 addition saturated polybutadiene, and B is also saturated polybutadiene but with 63% 1,2 addition. Because the polymers are rubbery and cannot be floated, a novel method was developed to create supported multilayer stacks. Dynamic SIMS was adopted to measure interfacial volume-fraction profiles of the diblock copolymer which are then compared with theoretical predictions based upon SCFT. The $\chi$ parameter and the statistical segment lengths were all determined previously from small-angle neutron scattering (SANS) from homogeneous, binary A/B homopolymer blends.[45] The molecular weights of the homopolymers used in the SANS experiments were considerably smaller than those used in the adsorption experiments. Since all the input parameters to the SCFT calculations are predetermined, rigorous comparisons can be made between experimental and theoretical results with no adjustable parameters. Three comparisons were made: the adsorption isotherm, the partition coefficient of the diblock copolymer between the two homopolymer phases, and the distribution of block copolymer segments at the A/B interface.

## Experimental Method

**Polymer Synthesis.** Polybutadiene was synthesized via anionic polymerization in hexane using tetrahydrofuran (THF) as a polar additive to control the percent of 1,2- vs 1,4-addition. All reagents were purified under high vacuum. A trial-and-error method was employed to develop a calibration curve for the dependence of the percent 1,2- and 1,4-addition on initiator (*sec*-butyllithium) concentration and molar ratio of THF to initiator. A diblock copolymer of polybutadiene, with a different percent 1,2-addition for each of the blocks, was synthesized by sequential polymerization, in which the THF concentration in the reactor was adjusted after completing the polymerization of the first block. An aliquot of the first block (precursor) was isolated and terminated for characterization purposes, prior to the addition of the second block. The polymers were dried fully under vacuum at room temperature until they reached constant weight. They were then saturated (in solution in cyclohexane) using either hydrogen or deuterium gas in a Parr high-pressure reactor at 95 °C with a 5% palladium on barium sulfate catalyst. The hydrogenated polymers were again dried under vacuum at 150 °C for several days. In this paper, we use the nomenclature sPB90 and sPB63 to describe saturated polybutadienes (with 90% and 63% 1,2-addition, respectively). The nomenclature hPB90/dPB90 and hPB63/dPB63 is used to distinguish between hydrogenated and deuterated polymers. Additional details of synthesis procedures can be found in ref 46.

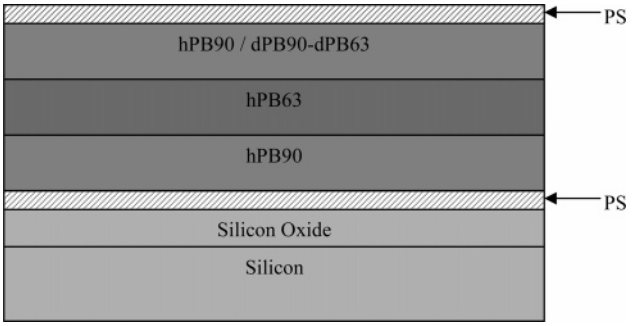


**Figure 1.** Diagram of the constructed polymer film.

**Table 1. Polymer Properties**

| polymer | $M_w$ (kg/mol$^{-1}$) | PDI | % 1,2 | $\rho$ (g cm$^{-3}$) |
|---|---|---|---|---|
| hPB90 homopolymer | 220 | 1.02 | 88 | 0.86 |
| hPB63 homopolymer | 187 | 1.02 | 63 | 0.86 |
| dPB63−dPB90 diblock copolymer | 38−41 | 1.02 | 63−92 | 0.91 |

**Polymer Characterization.** The molecular weights and architectures of the polymers were determined on a Waters 2690 gel permeation chromatography (GPC) system with a Viscotek triple detector. The three detectors (light scattering, viscometry, and refractometry) enabled the determination of the absolute number- and weight-averaged molecular weights ($\overline{M_n}$ and $\overline{M_w}$) and the polydispersity index (PDI) of the homopolymers and the block copolymer. The molecular weight of the block copolymer precursor was determined using only refractometry and an sPB calibration curve due to limited sample quantities. The refractive indices of the polybutadiene/THF solutions were independent of the percent of 1,2-addition in the range of our experiments; this simplification enabled the characterization of the block copolymer. NMR spectroscopy was used to determine the percent 1,2- and 1,4-addition in all of the samples to an accuracy of ±1%. An aliquot of the precursor of the diblock copolymer was analyzed by NMR. The extent of 1,2-addition of the second block was then determined from the known molecular weights of the precursor and diblock copolymer and the percent of 1,2-addition of the precursor. The pure diblock-copolymer melt was previously determined using small-angle neutron scattering to be disordered at room temperature,[47] in agreement with mean-field predictions ($\chi N = 10$, see Table 4). The two homopolymers are strongly immiscible ($\chi N = 25$, see Table 4). The characteristics of the polymers used in this study are summarized in Table 1. Labels for the polymers are based on our targets. Samples wherein the percent 1,2-addition deviated more than 2% from the targets were discarded.

**Film Preparation.** Most of the polymer films used in this investigation consisted of a trilayer of hPB90/hPB63/hPB90. The films were capped with 50 nm thick polystyrene (PS) layers on either side, as illustrated in Figure 1. The dPB90−dPB63 diblock copolymer was, in most cases, initially dissolved in the topmost hPB90 layer. The substrates used for the capped films were silicon wafers that had been oxidized for 2 h at 1000 °C in air to create a 90 nm layer of oxide on the surface prior to use. First, a 50 nm film of PS was spin-coated onto the oxidized silicon surface at 3000 rpm using a 0.5 wt % polymer solution in toluene. The PS film helped to prevent dewetting of the sPB films and also allowed for the construction of a symmetric film. The next sPB layer could not be directly spin-coated onto the PS film because this procedure would dissolve the polystyrene. It was also not possible to float an sPB film because the rubbery nature of the film caused it to shrivel on the surface of the water.[48] Instead, as portrayed in Figure 2, the sPB film was spin-coated onto a piece of freshly cleaved mica (3000 rpm using a 2 wt % polymer solution in toluene) and then transferred onto the PS-coated silicon wafer. The transferring technique used was an adaptation of that described by Scheffold et al.[48] One end of the piece of mica was dipped into a drop of water, held there for several seconds,

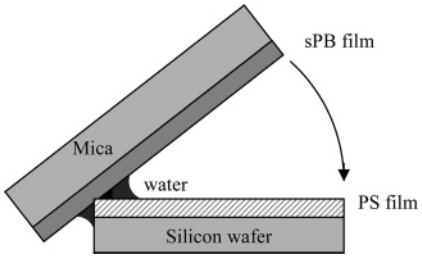


**Figure 2.** Schematic of the technique to transfer a rubbery polymer film from a piece of mica onto a PS-coated silicon wafer. The mica is gently lowered onto the silicon wafer, and a drop of water spreads between the two, transferring the rubbery polymer film from the mica onto the PS-coated silicon wafer.

removed with a small drop of water still clinging to the end, and set upright at the edge of the silicon wafer (Figure 2). The mica was then slowly lowered onto the silicon wafer until the mica and wafer touched. When the mica was peeled off, a smooth film of sPB remained on the PS film. The second and third sPB films were deposited in a similar manner. Finally, a 50 nm layer of PS was floated onto the top of the sandwich following a common practice in dynamic SIMS experiments.[41] The top and bottom sPB90 films were 150 nm thick while the center sPB63 film was either 150 or 300 nm thick. The films are labeled F[*xx*], where *xx* is the overall volume fraction of the A−B block copolymer in the three sPB layers of the film. The characteristics of the films used in this study are summarized in Table 2. The symbols included in Table 2 are those used to represent the data in Figures 11 and 14. Except in three films (F[0.091], F[0.121], and F[0.156]), the copolymer was initially confined to the top layer.

A Sentech SE400 ellipsometer was used to characterize the film thicknesses. Thicknesses of the actual films used were not measured, but rather films spun from the same solution onto silicon wafers were measured in their place. The thicknesses of the films, as spun onto the mica, were measured and controlled to within 2% of the target. However, some minor changes in the film thickness occurred during the process of transferring the films from the mica onto the silicon wafer.

All films were annealed at room temperature for at least 1 week before the SIMS measurements were made, since the dPB90−dPB63 diblock copolymer has to diffuse from the top hPB90 layer to the bottom hPB90 layer during equilibration.

**Secondary Ion Mass Spectrometry (SIMS).** The dynamic SIMS measurements discussed in this article were taken with a Physical Electronics 6650 instrument using a 3 kV, 60 nA beam of $O_2^+$ ions at 60° off normal incidence, which was rastered over a 0.04−0.09 mm$^2$ region. A static, defocused, 350−500 V electron beam was used for charge neutralization. Negative ions of H, D, C, and Si were monitored as a function of time from an electronically gated area that was 15% of the rastered area. At room temperature, the polymers under investigation were well above their glass transition temperature, so it was necessary to perform the SIMS measurements on a liquid nitrogen cooled cold stage which reached a temperature of approximately −100 °C. More details regarding SIMS depth profiling of polymers can be found in a review article by Schwarz et al.[41] Measurements were made on five different days spanning several months so that the ion-beam quality was not constant across all samples. The instrument parameters for the different days are given in Table 3.

## Theory

The free energy of mixing for the three components in our films is described by Flory−Huggins theory

$$\frac{Fv}{VkT} = \frac{\phi_A}{N_A}\ln\phi_A + \frac{\phi_B}{N_B}\ln\phi_B + \frac{\phi_{AB}}{N_{AB}}\ln\phi_{AB} + \chi[(\phi_A + f\phi_{AB})(\phi_B + (1-f)\phi_{AB}) - \phi_{AB}f(1-f)] \quad (1)$$

where $F/V$ is the free energy density of mixing, $v$ is the reference volume upon which $N$ and $\chi$ are based, $N$ is the number of reference volume units in a polymer chain, $\chi$ is the Flory−Huggins interaction parameter, $\phi$ is the volume fraction of a polymer species, and $f$ is the volume fraction of A monomers in the diblock copolymer. The subscripts A, B, and AB refer to the homopolymers A and B and the diblock copolymer AB. Although this equation is sufficient for describing the phase behavior of homogeneous blends, it cannot be used to describe nonhomogeneous regions such as an interface.

The interfacial composition profile between coexisting polymer phases containing block copolymers is predicted using one-dimensional self-consistent-field theory (SCFT).[38,49−51] Our methods for obtaining concentration profiles by SCFT are thoroughly described elsewhere.[45,46,52] The essence of SCFT is that the interactions between different polymers are replaced by interactions with equivalent external fields. With these proposed external fields, the volume-fraction profile of each polymer species is found that minimizes the free energy. Self-consistency then requires that the external fields, produced by these volume-fraction profiles, are consistent with the external fields originally proposed. Self-consistency is achieved by numerical iteration.

For the purposes of this work, the end result is the volume-fraction profile of the diblock copolymer, $\phi_{AB}(z)$, across the interface between two homopolymers, where $z$ is depth into the film. The volume-fraction profile depends on $\chi$, the two statistical segment lengths, $l_A$ and $l_B$, the chain lengths of the two homopolymers, $N_A$ and $N_B$, and the two blocks of the diblock copolymer, $N_{Ab}$ and $N_{Bb}$, and the overall composition of the film.

**Determination of Parameters for SCFT.** Room temperature (296 K) values of the $\chi$ parameter between sPB90 and sPB63 and the two statistical segment lengths used in the calculations were determined previously by fitting the random-phase approximation (RPA) to small-angle neutron scattering from binary homopolymer blends[45] and are given in Table 4. The determination of these parameters and their application to SCFT are discussed in ref 45. We assume that the value of $\chi$ between sPB90 and sPB63 is independent of the level of deuteration. This is reasonable given the magnitude of the $\chi$ parameter.[53,54] The self-consistent-field calculations thus contain no adjustable parameters.

**Reduction of SIMS Data.** A typical result from a dynamic SIMS measurement for one of the trilayer films is presented in Figure 3, corresponding to film F[0.069] in Table 2. The number of counts of H, D, C, and Si ions are given vs time for completeness, although only the H and D counts are used here. For a dynamic SIMS profile, sputtering time corresponds to depth into the film. The $t = 0$ edge in Figure 3 represents the upper surface of the top polystyrene layer, which is followed by the hPB90/hPB63/hPB90 trilayer, the bottom polystyrene layer, and finally the oxidized silicon substrate. Because the diblock copolymer is the only deuterated component in the film, the D counts reflect the concentration profile of diblock copolymer through the film. The extremely low D counts in the two PS layers of Figure 3 show that the diblock copolymer is confined to the sPB trilayer, while the two peaks confirm positive adsorption of the diblock copolymer at the two hPB90/hPB63 interfaces. To remove artifacts due to charging (notice the drift in the C and H counts in Figure 3), the

**Table 2. Films Examined**

| day | symbols used in Figures 11 and 14: upper interface | symbols used in Figures 11 and 14: lower interface | name | thickness (nm): top A | thickness (nm): middle B | thickness (nm): bottom A | initial volume fraction of diblock copolymer: top A | initial volume fraction of diblock copolymer: middle B | initial volume fraction of diblock copolymer: bottom A |
|---|---|---|---|---|---|---|---|---|---|
| 1 | ○ | | F[0.025] | 150 | 150 | 0 | 0.050 | 0 | 0 |
| | ○ | | F[0.053] | 150 | 150 | 0 | 0.105 | 0 | 0 |
| | ○ | | F[0.101] | 150 | 150 | 0 | 0.201 | 0 | 0 |
| | NE[a] | | F[0.196] | 150 | 150 | 0 | 0.391 | 0 | 0 |
| 2 | △ | △ | F[0.016]a | 150 | 150 | 150 | 0.049 | 0 | 0 |
| | △ | △ | F[0.016]b | 150 | 150 | 150 | 0.049 | 0 | 0 |
| | △ | △ | F[0.016]c | 150 | 150 | 150 | 0.049 | 0 | 0 |
| | △ | △ | F[0.035] | 150 | 150 | 150 | 0.105 | 0 | 0 |
| | NE | + | F[0.130] | 150 | 150 | 150 | 0.391 | 0 | 0 |
| 3 | ● | ● | F[0.007] | 150 | 300 | 150 | 0.029 | 0 | 0 |
| | ● | ● | F[0.022] | 150 | 300 | 150 | 0.086 | 0 | 0 |
| | ● | ● | F[0.043] | 150 | 300 | 150 | 0.173 | 0 | 0 |
| | ● | ● | F[0.057] | 150 | 300 | 150 | 0.227 | 0 | 0 |
| | ● | ● | F[0.069] | 150 | 300 | 150 | 0.274 | 0 | 0 |
| | ◇ | ◇ | F[0.091] | 150 | 300 | 150 | 0.182 | 0 | 0.182 |
| 4 | ◇ | ◇ | F[0.121] | 150 | 300 | 150 | 0.242 | 0 | 0.242 |
| | NE | NE | F[0.156] | 270 | 300 | 270 | 0.242 | 0 | 0.242 |
| 5 | ● | ● | F[0.0003] | 150 | 300 | 150 | 0.0012 | 0 | 0 |
| | ● | ● | F[0.0015] | 150 | 300 | 150 | 0.0060 | 0 | 0 |
| | ● | ● | F[0.0027] | 150 | 300 | 150 | 0.0107 | 0 | 0 |
| | ● | ● | F[0.0053] | 150 | 300 | 150 | 0.0210 | 0 | 0 |

[a] NE = nonequilibrated interface.

**Table 3. SIMS Parameters**

| day | current (nA) | voltage (kV) | area ($\mu m^2$) | gate (%) | etch rate, nm $s^{-1}$: mean | etch rate, nm $s^{-1}$: st dev |
|---|---|---|---|---|---|---|
| 1 | 60 | 3 | 200 × 200 | 15 | 0.806 | 0.060 |
| 2 | 60 | 3 | 250 × 250 | 15 | 0.542 | 0.010 |
| 3 | 60 | 3 | 250 × 250 | 15 | 0.548 | 0.022 |
| 4 | 60 | 3 | 300 × 300 | 15 | 0.327 | 0.009 |
| 5 | 60 | 3 | 200 × 200 | 15 | 0.771 | 0.042 |

**Table 4. SCFT Parameters[a]**

| | | | |
|---|---|---|---|
| $\chi$ | 0.00642 | $N_B$ | 3600 |
| $l_A$ | 0.491 nm | $N_{Ab}$ | 790 |
| $l_B$ | 0.749 nm | $N_{Bb}$ | 730 |
| $N_A$ | 4230 | | |

[a] $l$ is the statistical segment length, $N$ is the number of reference unit volumes in a polymer, A is sPB90, B is sPB63, and Ab and Bb are the respective blocks of the diblock copolymer. All parameters are based upon a reference volume of 100 $Å^3$.

deuterium counts were normalized by the sum of both deuterium and hydrogen counts, D/[D + H]. This ratio was then adjusted to account for deuterium counts from the homopolymers (D/[D + H] = 0.000 57 for hPB63 and 0.000 19 for hPB90, as compared to the natural abundance of 0.000 12) and normalized with a conversion factor such that the total calculated volume fraction of the diblock copolymer in the film matched the known overall concentration. To convert sputter time to depth, a mean etch rate for each day's analysis was calculated from the target thicknesses of the sPB layers. These mean etch rates are listed in Table 3 along with the standard deviations of the calculated etch rates.

Once the D/[D + H] ratio has been converted to the volume fraction of diblock copolymer, $\phi_{AB}(t)$, and the sputtering time has been converted to film depth, a volume-fraction profile can be constructed, $\phi_{AB}(z)$. A typical volume-fraction profile thus obtained is shown in Figure 4 for film F[0.069]. $\phi_{AB}(z)$ is the volume fraction of diblock copolymer, and $z$ represents depth through the film where the origin is at the vacuum/PS surface. It is clear that our normalizing procedure removes the drift that is evident in Figure 3.

The relationship between the actual volume-fraction profile of the diblock copolymer through the film, $\phi_{AB}(z)_{actual}$, and the measured volume-fraction profile, $\phi_{AB}(z)_{SIMS}$, is determined by convolution with the instrument resolution function $R(z)$, as follows:

$$\phi_{AB}(z)_{SIMS} = R(z)\phi_{AB}(z)_{actual} = \int dx\, R(x)\phi_{AB}(z+x)_{actual} \quad (2)$$

where $R(z)$ is normalized such that $\int dz\, R(z) = 1$. The integral is taken over the region where $R(z)$ is nonzero (−100 to 100 nm). The instrumental resolution was determined from measurements of sharp homopolymer/homopolymer interfaces as described in Appendix A and is given in Figure 5. We assume for simplicity that the instrumental resolution function is independent of particular location within the film.

## Results and Discussion

Upon returning to the data obtained from film F[0.069] shown in Figure 4, we see that while there is clearly positive adsorption at the two hPB90/hPB63 interfaces, the diblock copolymer is not adsorbed at the two PS/hPB90 interfaces. When the sample was prepared, all of the diblock copolymer in F[0.069] was initially in the upper hPB90 layer. After annealing the sample for 1 week at room temperature, the diblock copolymer is distributed throughout the trilayer stack. Redistribution requires that, the diblock copolymer molecules diffuse across the two hPB90/hPB63 interfaces and the intervening hPB63 layer. The equality of $\phi_{AB}$ in the top and bottom hPB90 layers, the symmetry of the adsorption peaks, and the constant block copolymer concentration attained in the middle hPB63 layer provide unambiguous proof that our systems are at equilibrium.

The only films showing qualitatively different behavior to that shown in Figure 4 were films F[0.196], F[0.156], and F[0.130]. An example is shown in Figure 6, which plots the volume-fraction profile of the diblock copolymer for film F[0.130]. The peak in the diblock copolymer concentration in the top hPB90 layer is

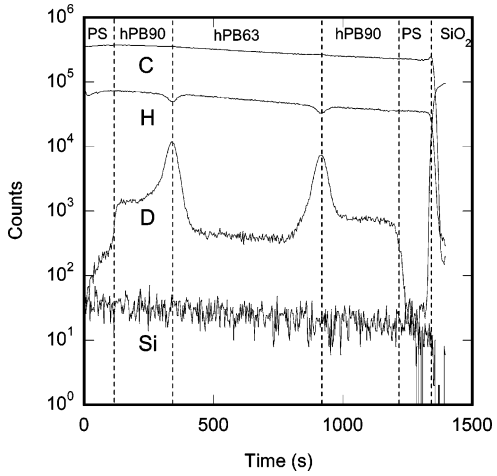


**Figure 3.** Raw dynamic SIMS data for film F[0.069]. Number of counts in each collection interval for four ions: carbon (C), hydrogen (H), deuterium (D), and silicon (Si). Vertical dashed lines demark the interfaces between the various layers shown in Figure 1.

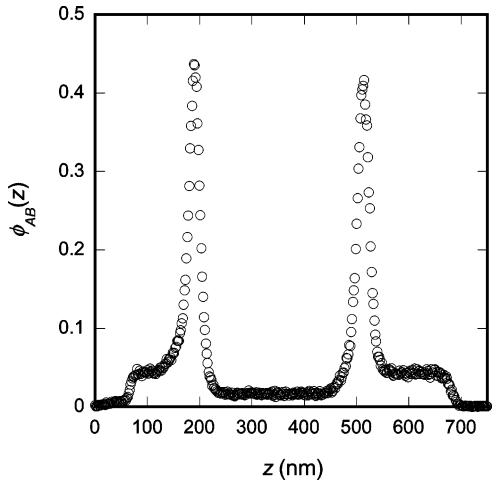


**Figure 4.** Measured volume fraction profile of diblock copolymer across film F[0.069].

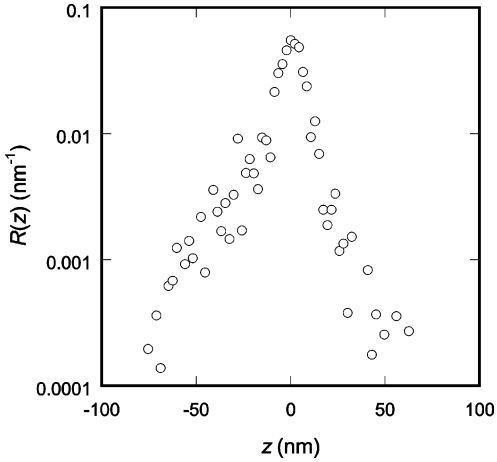


**Figure 5.** Instrumental resolution function derived from the hPB90/dPB63 and dPB63/hPB90 bilayers shown in Figure 15a.

believed to be a result of phase separation of the initial diblock copolymer/homopolymer blend. It appears in Figure 6 that the second interface is equilibrated so data from this second interface in F[0.130] are included in later plots. Film F[0.196] contained only one sPB90/sPB63 interface (the film contained an sPB bilayer

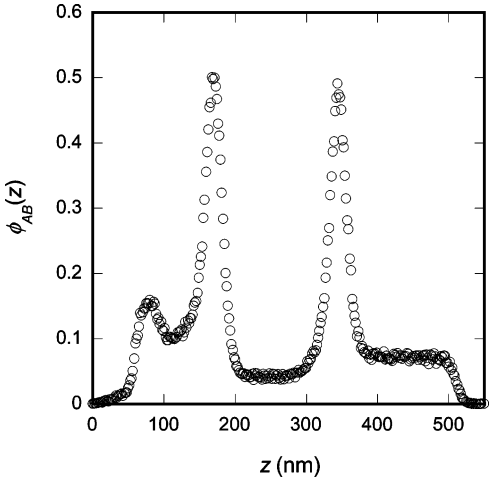


**Figure 6.** Measured volume fraction of diblock copolymer across film F[0.130]. The left-most peak is attributed to phase separation of the diblock copolymer from the homopolymer in the upper hPB90 layer.

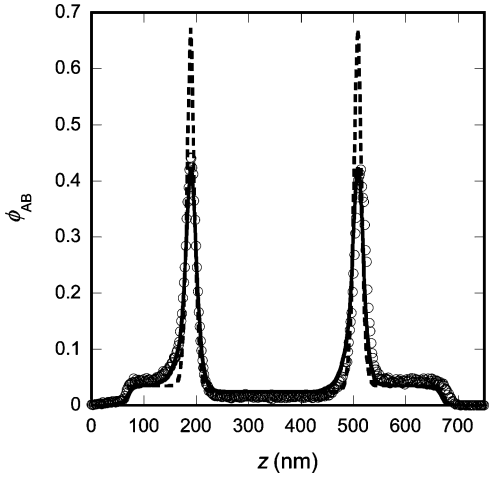


**Figure 7.** Measured volume fraction profile of diblock copolymer across film F[0.069] (open circles) with the unconvoluted SCFT calculated volume fraction profile (dashed line) and the SCFT calculated volume fraction profile convoluted with the instrumental resolution function (solid line).

rather than a trilayer); thus, data from this film will not be used. In film F[0.156], diblock copolymer was initially loaded into both the top and bottom films so that both interfaces were affected by nonequilibrated behavior. The initial volume fraction of diblock copolymer in the top layers of these nonequilibrating films were 0.391 for F[0.196] and F[0.130] and 0.242 for F[0.156] (see Table 2). The well-equilibrated films with the highest initial concentration of diblock copolymer in their top layers were films F[0.121], F[0.069], and F[0.057] with initial volume fractions of 0.242, 0.274, and 0.227, respectively. It is clear that at an initial diblock copolymer volume fraction of around 0.25 there is a crossover from films that are equilibrated to ones where nonequilibrating behavior is seen.

Self-consistent-field theory was used to generate theoretical volume-fraction profiles of the diblock copolymer across the trilayer to compare with those determined experimentally. The initial guess required to start the SCFT iteration process was chosen such that the two hPB90 layers have roughly the correct thicknesses (see Table 2). Figure 7 compares the theoretical predictions with the experimental results for film F[0.069]. Figure 8a provides a close-up view on a

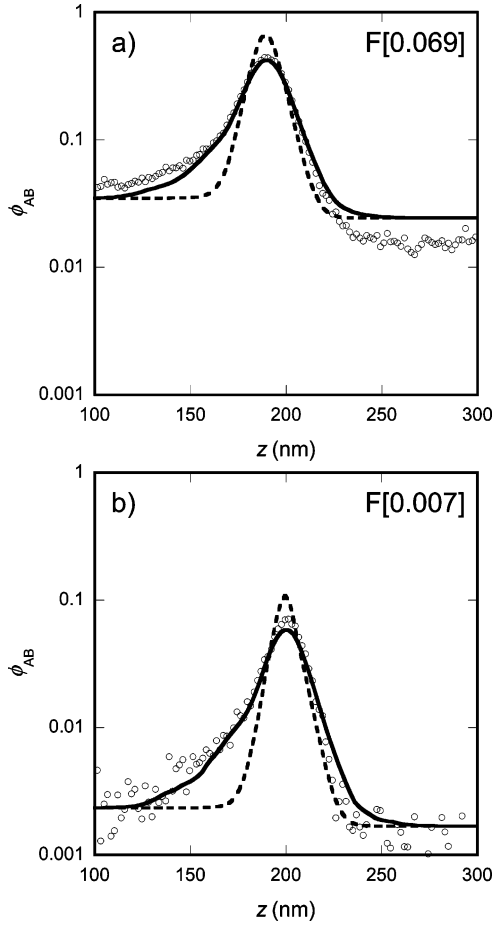


**Figure 8.** Volume fraction profiles of the diblock copolymer across the interface between the two homopolymers for films (a) F[0.069] and (b) F[0.007]. Open circles are the reduced SIMS data points, the dashed line is the prediction from self-consistent-field theory, and the solid line is the SCFT prediction convoluted with the proposed instrumental resolution function.

logarithmic scale of the left interface in Figure 7, and Figure 8b is the equivalent plot for a trilayer film with an order of magnitude less diblock copolymer, F[0.007]. The experimental data points are presented as open circles while the uncorrected theoretical SCFT profile is represented by a dashed line. The SCFT profile is shifted such that the first peak position matches the experimental data. The solid line represents the theoretical interfacial profile convoluted with the instrumental resolution function. In Figure 8a, the fit around the peak shows remarkable agreement between theory and experiment. There is, however, a discrepancy in the volume fractions of diblock copolymer in the bulk, away from the interface. Theory incorrectly predicts the partition coefficient of the diblock copolymer between the two polymer layers. This discrepancy could be due to an error in our measurement of the diblock copolymer symmetry, $f$, or it could be due to the application of an independently determined parameter measured from a 50/50 blend of two homopolymers to the dilute limit where the volume fraction of the diblock copolymer in the bulk phases is only 0.02. Figure 8b shows similar behavior, but assessment of agreement between theory and experiment away from the peak is difficult due to the experimental noise. The success of the resolution function (Figure 5) obtained from the homopolymer bilayer experiments is also worth noting. The agreement between experiment and theory at the PS/hPB90 interfaces (Figure 7, $z = 50$ and 700 nm), where the volume fraction of diblock copolymer drops abruptly, is entirely due to the resolution function. The SCFT calculations do not explicitly model these interfaces. Rather, they are treated as reflective boundary conditions.

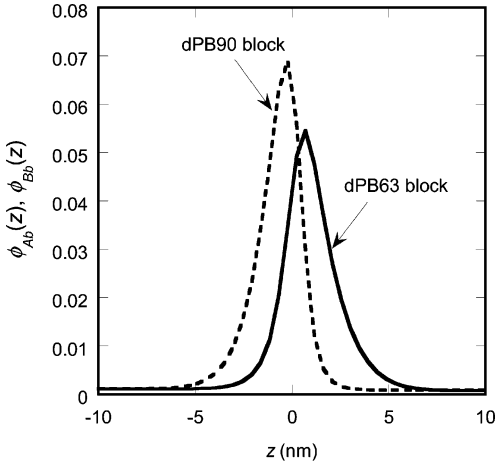


**Figure 9.** Volume-fraction profiles for the A and B blocks of the diblock copolymer across a homopolymer/homopolymer interface predicted from SCFT. The dashed and solid lines are the volume fraction profiles for the sPB90 (A) and sPB63 (B) blocks of the diblock copolymer, respectively.

The SCFT calculations provide additional insight into the nature of the adsorbed layer that is not provided by our SIMS experiments. Figure 9 shows the volume-fraction profiles of the two blocks of the sPB63−sPB90 copolymer separately as calculated by SCFT. The origin of the surfactancy of the amphiphilic diblock copolymers is evident from this plot. The sPB90 block of the diblock copolymer extends from the interface (at $z = 0$) into the sPB90 homopolymer, and the sPB63 block of the diblock copolymer extends into the sPB63 homopolymer. The difference in height between the two peaks is a manifestation of the large difference between the statistical segment lengths of sPB90 and sPB63, which are 0.49 and 0.75 nm, respectively (based on a reference volume unit of 100 Å$^3$).[45]

The agreement between theory and experiment, seen in Figures 7 and 8, applies to all of the films that were studied. Equilibrium adsorption is adequately characterized by four parameters: the volume fraction of diblock copolymer in the hPB90 film, $\phi_{AB/A}$, the volume fraction of diblock copolymer in the hPB63 film, $\phi_{AB/B}$, the amount of diblock copolymer adsorbed at the interface, $\Gamma$, and the width of the diblock copolymer volume-fraction peak, $\sigma$. Calculation of $\Gamma$ is based on the Gibbsian surface, as pictured for the F[0.069] film in Figure 10. The nominal location of the Gibbs dividing surface was chosen to be the position of the peak in the volume-fraction profile. Then $\Gamma$, which has units of nanometers (volume of diblock copolymer per unit area), is given by the hatched area in Figure 10. Also defined in Figure 10 are $\phi_{AB/A}$ and $\phi_{AB/B}$, the diblock copolymer concentrations in the two surrounding bulk phases, sufficiently far away from the interface.

Parts a and b of Figure 11 plot $\Gamma$ as a function of $\phi_{AB/A}$ and $\phi_{AB/B}$, respectively. The symbols represent measurements from the various films listed in Table 2, whereas the curves represent SCFT predictions. The solid curve gives the theoretical predictions using $\chi = 0.0064$, $l_{sPB90} = 0.49$ nm, and $l_{sPB63} = 0.75$ nm, obtained from SANS (all parameters are based on a reference volume

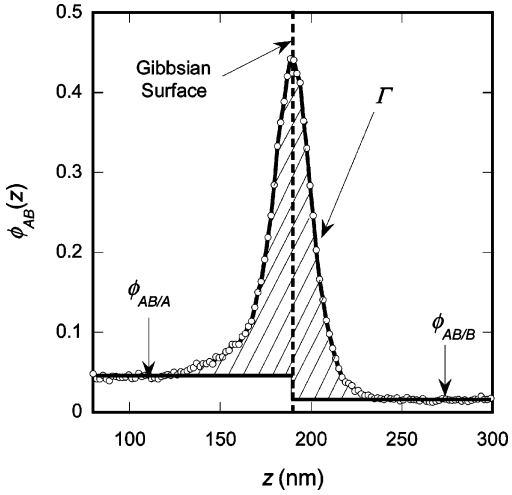


**Figure 10.** Volume fraction of diblock copolymer through an hPB90/hPB63 interface for film F[0.069]. The crosshatched area represents the adsorbed amount, Γ.

of 100 Å$^3$). The theoretical adsorption isotherm is a sensitive function of the $\chi$ parameter. This is depicted by the upper and lower dashed curves in parts a and b of Figure 11, which represent adsorption isotherms for $\chi$ at 0.0070 and 0.0058, respectively, corresponding to $\pm 10\%$ deviations from the measured value. The maximum value of $\phi_{AB/A}$ that is allowed theoretically is 0.083 (for $\chi = 0.0064$), as indicated by the vertical dashed line in Figure 11a. This value is the concentration of diblock copolymer at the binodal and thus demarks the change from a stable to a metastable mixture. Similarly, the maximum value of $\phi_{AB/B}$ that is allowed theoretically is 0.054 (Figure 11b). When $\phi_{AB/A}$ reaches 0.083 (or, equivalently, $\phi_{AB/B}$ reaches 0.054), theory predicts the formation of a separate homogeneous block copolymer-rich phase (method of common tangent planes with the Flory−Huggins equation, eq 1). This behavior is seen in the solid lines in Figure 11a,b as a sharp upward turn in the adsorption isotherm. In Appendix B, we show that at the binodal ($\phi_{AB/A} = 0.083$) an interfacial monolayer of diblock copolymer exists in equilibrium with a bulk homogeneous diblock copolymer-rich phase. Thus, adsorbed amounts greater than the adsorption isotherm's first intercept of the binodal in Figure 11 correspond to SCFT solutions that are not thermodynamically stable (analogous to the binodal region of the van der Waals equation of state). Nevertheless, we include these unstable and metastable solutions in the plots for completeness. It is evident that the dependences of Γ on $\phi_{AB/A}$ and $\phi_{AB/B}$ obtained by theory and experiment are in excellent agreement. At very low concentrations of diblock copolymer, the correction for background deuterium is of the same magnitude as the amount of deuterium from the diblock copolymer. $\phi_{AB/A}$ and $\phi_{AB/B}$ are, thus, very sensitive to this background correction. The slight discrepancy between experiment and theory at low concentrations of diblock copolymer in Figure 11a is most likely due to this sensitivity. In Figure 11b, $\phi_{AB/B}$ was calculated to be less than zero for a number of films with very low diblock copolymer concentrations (i.e., detected deuterium counts were lower than the proposed background). These points are not included in Figure 11b. We note that the adsorption isotherm does not depend on factors such as film thickness or where the block copolymer was placed initially.

We define $\sigma$ to be the width of the interfacial peak in the diblock copolymer volume-fraction profile. $\sigma$ was

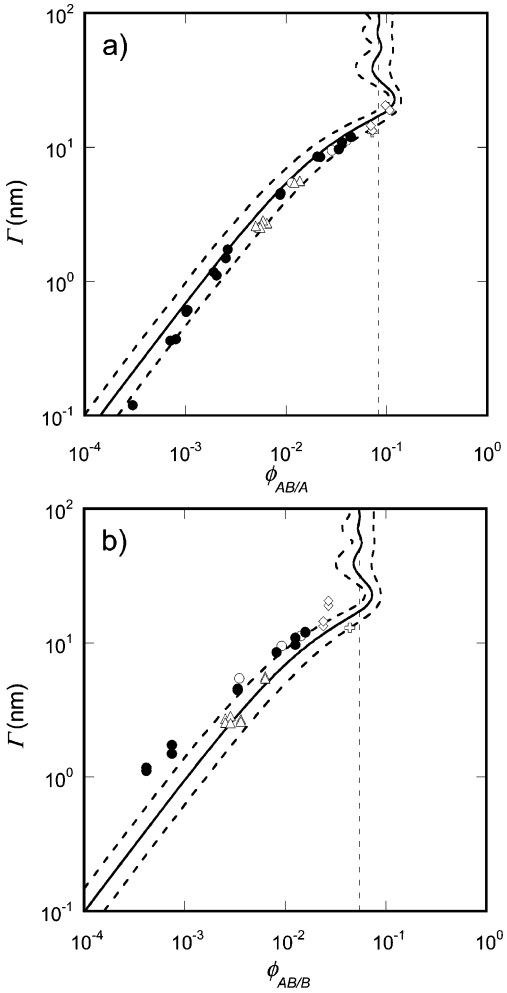


**Figure 11.** Adsorption isotherms. The dependence of the adsorbed amount, Γ, on (a) $\phi_{AB/A}$ and (b) $\phi_{AB/B}$. Three SCFT theoretical isotherms are plotted along with the experimental SIMS data. The solid line corresponds to theory using the $\chi$ value of 0.0064 previously determined while the two dashed lines were calculated using $\chi$ values of 0.0058 and 0.0070. The vertical dashed line denotes the concentration of diblock copolymer at which formation of a diblock copolymer-rich phase is predicted. Correspondence between the different symbols and the different films is shown in Table 2.

found by fitting a Gaussian curve to the upper half of the volume-fraction peak (e.g., Figure 10) and setting $\sigma$ to the fitted standard deviation. Widths for the SIMS adsorption peaks (open circles in Figure 8) are plotted in Figure 12 against the amount of diblock copolymer adsorbed and have been corrected for the effects of instrumental resolution. The results from the upper hPB90/hPB63 interface are given by the filled diamonds while the results from the lower hPB63/hPB90 interface are given by open diamonds. Widths for the SCFT calculations (dashed curves in Figure 8) were calculated in the same manner and are given in Figure 12 by the dashed line. To compare these theoretical widths with the experimental ones, it is necessary to take into account the effects of capillary-wave broadening. Since the interfacial tension decreases with increasing adsorbed diblock copolymer, the amount of capillary broadening is predicted to increase with adsorbed amount. Capillary broadening is given by

$$\langle \Delta\zeta^2 \rangle = \frac{kT}{2\pi\gamma} \ln\left(\frac{\lambda_{max}}{\lambda_{min}}\right) \quad (3)$$

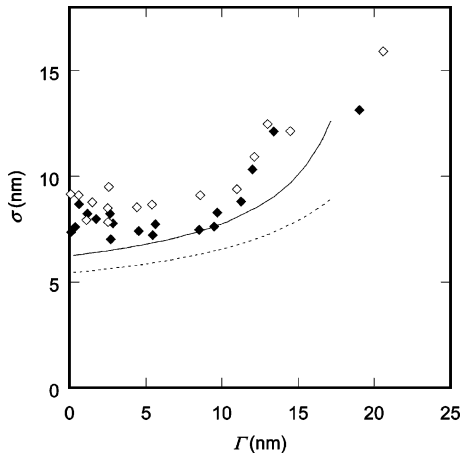


**Figure 12.** Width (standard deviation) of the volume fractions peaks plotted vs the amount adsorbed. Filled diamonds are experimental widths from the upper hPB90/hPB64 interfaces while the open diamonds are experimental widths from the lower hPB90/hPB64 interfaces. All experimental data have been corrected for the effects of instrumental resolution. The lower dashed line gives the widths of the volume-fraction peaks calculated using SCFT. The solid line modifies these theoretical widths to include the predicted effects of capillary waves. The two lines terminate at the binodal.

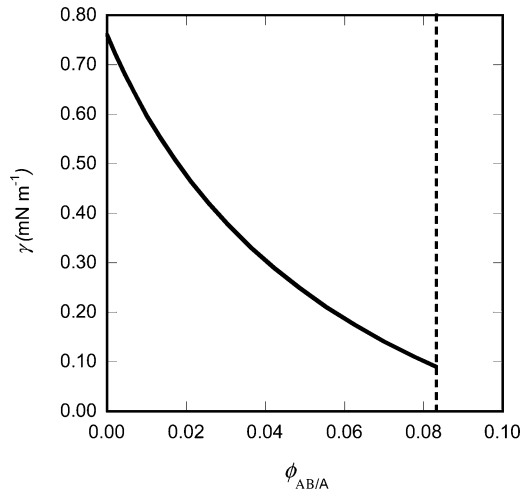


**Figure 13.** Interfacial tension, $\gamma$, is plotted against $\phi_{AB/A}$. The solid line gives the interfacial tension calculated by SCFT, and the vertical dashed line indicates the binodal concentration of diblock copolymer. The interfacial tensions for adsorbed diblock copolymer amounts greater than 17 nm are not included, since these do not correspond to thermodynamically stable solutions (see Appendix B).

where $\sqrt{\langle\Delta\zeta^2\rangle}$ is the rms amplitude of capillary fluctuations, $\gamma$ is the interfacial tension, and $\lambda_{max}$ and $\lambda_{min}$ are the maximum and minimum wavelengths of fluctuations.[55,56] We use $\lambda_{max} = 200\ \mu$m (the size of the SIMS crater) and $\lambda_{min} = 3$ nm (the width of the homopolymer/homopolymer interface). The interfacial tension is calculated using SCFT as described in ref 45. Figure 13 plots the interfacial tension, calculated from SCFT, against the volume fraction of diblock copolymer in the A homopolymer phase. The vertical dashed line in Figure 13 indicates the binodal block copolymer concentration. The final predicted width including the effects of capillary broadening is given in Figure 12 as the solid line. It was mentioned earlier that the experimentally measured volume-fraction profile peak widths were corrected for the effects of instrumental resolution. The measured instrumental resolution function is shown in Figure 5 and has a peak width of 6.6 nm. However, this resolution function was measured by profiling a homopolymer/homopolymer interface with some finite thickness (3.2 nm from SCFT) and predicted capillary broadening (3.1 nm). The actual instrumental resolution is thus $(6.6^2 - 3.2^2 - 3.1^2)^{1/2} = 4.9$ nm, and it is this number that is used to correct the experimental data.

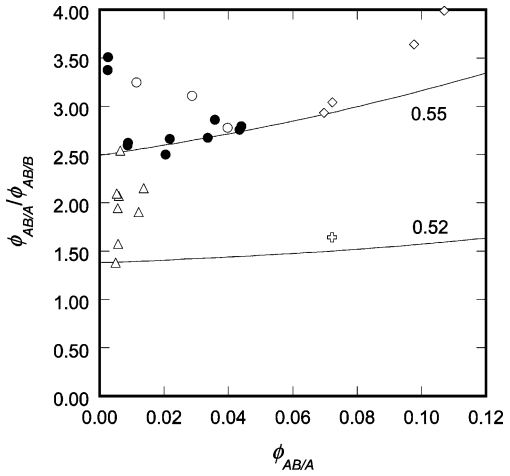


**Figure 14.** Partition coefficient, $\phi_{AB/A}/\phi_{AB/B}$, of the diblock copolymer between the two homopolymer phases is plotted against $\phi_{AB/A}$. The two solid lines indicate the ratio predicted from the Flory–Huggins model with the hPB90 fraction of the diblock copolymer, $f$, being 0.52 or 0.55.

The experimental results in Figure 12 show that the width of the adsorbed block copolymer layer increases from 8 to 14 nm as the adsorbed amount increases from 0 to 20 nm. Theory predicts an increase from 6 to 13 nm as the adsorbed amount increases from 0 to 17 nm (the upper limit set by the binodal). The fact that the SCFT calculations predict this trend in the layer thickness with independently determined $\chi$, $l_i$, and $N_i$ parameters is a remarkable demonstration of the robustness of the experimentally determined parameters and the theoretical constructs developed to characterize polymer interfaces. In Figure 12, the experimental peak widths from the lower hPB90/hPB63 interface (open diamonds) give widths slightly larger than the peak widths of the upper interface (filled diamonds). This is probably due to the dependence of the instrumental resolution function on depth which we ignored.

In Figure 14 we plot the partition coefficient of diblock copolymer between the two coexisting phases, $\phi_{AB/A}/\phi_{AB/B}$, against $\phi_{AB/A}$. The experimental data do not support a clear trend for the dependence of $\phi_{AB/A}/\phi_{AB/B}$ on $\phi_{AB/A}$. Instead, the data are scattered between 1.5 and 3.5. The expected value of $\phi_{AB/A}/\phi_{AB/B}$ (the partition coefficient) is calculated from Flory–Huggins theory (eq 1), since it is not a property of the interface. For a binary polymer blend, the phase-equilibrium calculation is solved by the common-tangent method. For a ternary polymer blend, the problem is essentially the same, but the tangent lines are now planes. The calculated $\phi_{AB/A}/\phi_{AB/B}$ ratio is a sensitive function of the block copolymer asymmetry, $f$. Theoretical predictions are shown (solid curves) for $f = 0.52$, the measured value, and $f = 0.55$. The experimental data are in better agreement with the $f = 0.55$ curve. This may be due to the finite polydispersity of our sample or error in our calculation of the diblock-copolymer asymmetry, $f$. In any case, the deviations between theory ($f = 0.52$) and experiment are not large, especially when one considers

the fact that the actual concentrations of the block copolymer in the bulk phases are lower than 2% in most of the films.

We conclude this section by addressing the behavior of the films at high diblock copolymer loadings. In films F[0.196], F[0.156], and F[0.130], a nonequilibrating peak in the diblock copolymer concentration was observed where the block copolymer was initially loaded (Figure 6). These peaks were seen when the initial volume fraction of diblock copolymer in the top layer approached 0.25. The room temperature spinodal for a binary blend of sPB90 and sPB63-sPB90 is at $\phi_{AB} = 0.249$ (i.e., the second derivative of the free energy with volume fraction is set to zero). It therefore seems possible that the nonequilibrating peaks observed at high diblock copolymer loadings are the result of macrophase separation in the bulk by spinodal decomposition.

The behavior predicted by SCFT at high diblock copolymer loadings is a monolayer of diblock copolymer at the homopolymer/homopolymer interface in coexistence with a third block copolymer-rich phase. This is established by comparing the interfacial tensions of different interfacial phases (monolayer, trilayer, etc.) as discussed in Appendix B. From a practical perspective, the reduction of the interfacial tension is important. Figure 13 plots the interfacial tension, calculated from SCFT, against the volume fraction of diblock copolymer in the A homopolymer phase. The interfacial tension at the binodal (vertical dashed line), calculated from SCFT ($\gamma = 0.09$ mN m$^{-1}$), is the minimum realizable tension and corresponds to an 89% reduction of the interfacial tension with no diblock copolymer present ($\gamma = 0.76$ mN m$^{-1}$). Addition of diblock copolymer thus enhances compatibilization up to a volume fraction of around 0.05−0.08 (depending on the relative amounts of the two homopolymers), after which additional diblock copolymer does not lower the interfacial tension but initiates a separate diblock copolymer-rich phase.

## Conclusions

We performed dynamic SIMS experiments to study the adsorption of a diblock copolymer to a polymer/polymer interface. The polymer system under investigation consists of three polymers: a saturated polybutadiene with 90% 1,2-addition (hPB90) homopolymer, a saturated polybutadiene with 63% 1,2-addition (hPB63) homopolymer, and a deuterated dPB90−dPB63 diblock copolymer. Thin films were constructed and annealed for a week at room temperature. Experimental data were compared with self-consistent-field theory (SCFT) calculations using the statistical segment lengths and a Flory−Huggins interaction parameter obtained previously from small-angle neutron scattering of binary homopolymer blends. Good agreement between the SCFT predictions and experimental measurements was obtained without adjustable parameters.

More quantitative comparisons between theory and experiment were made by describing the volume-fraction profiles with four parameters: the amount adsorbed at the interface, $\Gamma$, the width of the peak at the interface, $\sigma$, the volume fraction of diblock copolymer in the hPB90 layer, $\phi_{AB/A}$, and the volume fraction in the hPB63 layer, $\phi_{AB/B}$. The adsorption isotherms, $\Gamma$ vs $\phi_{AB/A}$ and $\Gamma$ vs $\phi_{AB/B}$, show good agreement between the measured isotherms and those predicted with SCFT. The width of the interfacial diblock copolymer volume-fraction peak, $\sigma$, is quantitatively in agreement with SCFT at low adsorbed amounts and qualitatively shows the same increase in width predicted with increasing adsorbed amount, $\Gamma$. The measurement of the partition coefficient, $\phi_{AB/A}/\phi_{AB/B}$, on $\phi_{AB/A}$ is in reasonable agreement with the SCFT calculations.

Although the more practically useful interfacial tension was not measured in this study, it can be calculated using SCFT, so that if the adsorption isotherm is successfully predicted by SCFT, then we can be confident in our theoretical calculations of the interfacial tension. Studies of polymer compatibilization can thus take advantage of the predictive powers of self-consistent-field theory using parameters derived from scattering from homogeneous polymer blends.

**Acknowledgment.** Financial support was provided by the National Science Foundation (CTS-0305711). The support and advice of Rachel Segalman and Edward Kramer are greatly appreciated. This work made use of MRL Central Facilities supported by the MRSEC Program of the National Science Foundation under Award No. DMR00-80034.

## Appendix A. SIMS Resolution Function

The secondary-ion mass spectrometer instrumental resolution, $R(z)$, was quantified by measuring the profiles of hPB90/dPB63 and dPB63/hPB90 films deposited on oxidized Si. These films were simple bilayers of the two homopolymers with no diblock copolymer added, but with the homopolymer dPB63 labeled with deuterium. The sPB bilayers were capped both above and below by PS films. The measured interfacial profiles from the films are shown in Figure 15 as open circles. $\phi_B(z)$ is the volume-fraction profile of the dPB63 homopolymer through the film. For convenience, the origin ($z = 0$) is located at the interface. The theoretical SCFT interfacial profiles are plotted in Figure 15 as dashed lines. Although the films themselves are 400 nm thick, only the central 200 nm is included in the figures for clarity. The difference between the theoretical interfacial profile and that measured using SIMS is accounted for by $R(z)$, assuming that the SCFT calculations provide an accurate representation of the actual homopolymer interfacial volume-fraction profile. Because the theoretical interfacial profile is much sharper than the experimental interfacial profile, the extraction of $R(z)$ is greatly simplified by assuming that the actual interfacial profile is a step function. With this simplification, $R(z)$ is simply the derivative of the measured interfacial profile. From Figure 15a we accurately find the derivative of the measured profile for $z < 0$. However, finding the gradient for $z > 0$ is more difficult because the volume fraction is essentially unity. For this reason the data in Figure 15b are used to construct the right half of the resolution function ($z > 0$), and Figure 15a is used for the left half ($z < 0$). The resultant, normalized resolution function, $R(z)$, is presented in Figure 5. The solid lines in Figure 15 represent the convolution of the theoretical interfacial profile calculated from SCFT (dashed lines) with $R(z)$. The excellent agreement between the experimental and convoluted interfacial profiles is not surprising since the instrumental resolution function was based on these measurements. It is worth noting that the shape of the instrumental resolution function reported here (Figure 5) is different from that usually observed in SIMS experiments.[57] The left-side tail is larger than the right-side tail, implying that

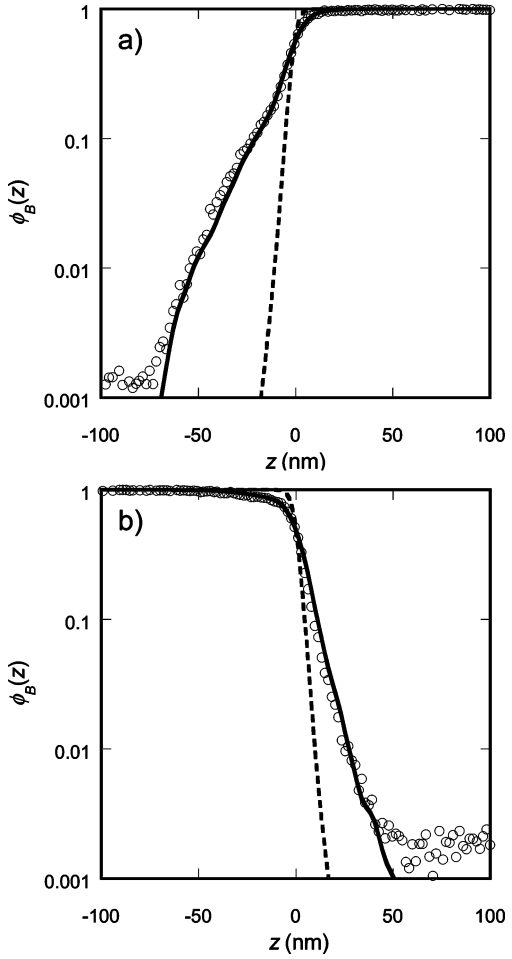


**Figure 15.** Experimental (circles) and theoretical (dashed line) interfacial profiles of an (a) hPB90/dPB63 interface and a (b) dPB63/hPB90 interface. The solid line represents the theoretical profile convoluted with the proposed instrumental resolution function.

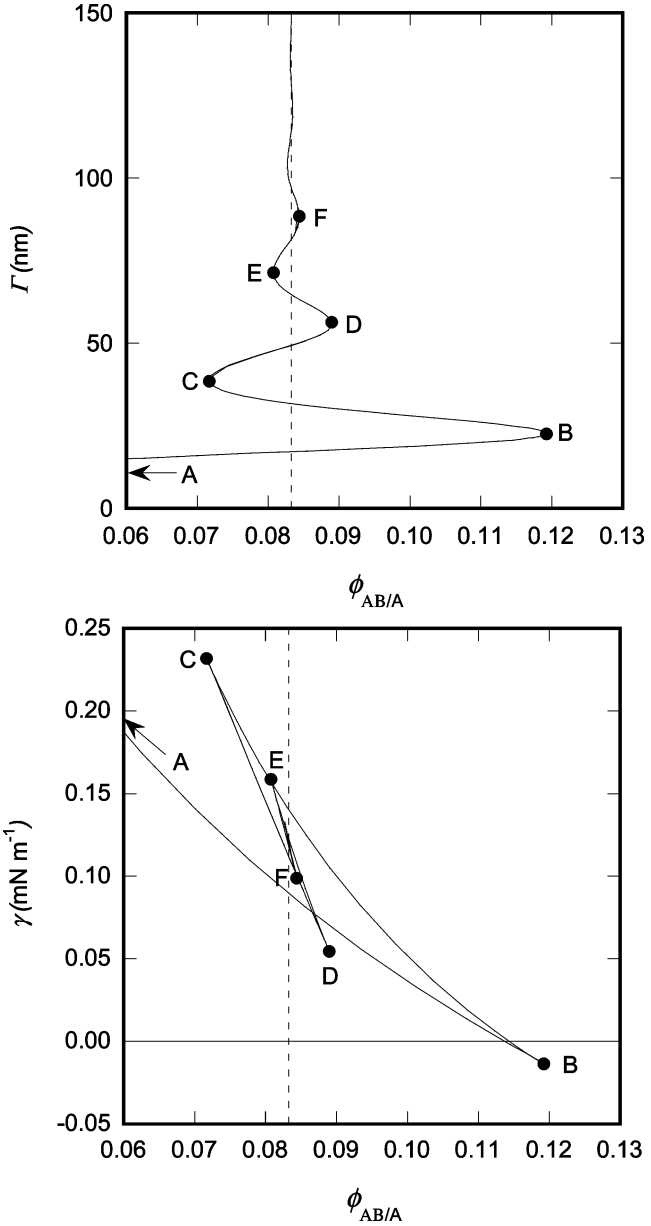


**Figure 16.** (a) Adsorbed amount of diblock copolymer, Γ, is plotted against the volume fraction of the diblock copolymer in the A homopolymer layer. A labels the point at $\phi_{AB/A} = 0$ of the adsorption isotherm, while B through F label the extrema and correspond to those in (b). The vertical dashed line indicates the value of $\phi_{AB/A}$ at the binodal. (b) Interfacial tension, $\gamma$, is plotted against the volume fraction of the diblock copolymer in the A homopolymer layer. A labels the point at $\phi_{AB/A} = 0$, while B through F label the extrema and correspond to those in (a). The vertical dashed line indicates the value of $\phi_{AB/A}$ at the binodal.

polymer fragments tend to diffuse up into layers above them more than they diffuse down into lower layers. One possible explanation for this is that the ion beam heats the surface, creating a temperature gradient through the film and warming the surface above the glass transition temperature. This temperature gradient results in a varying diffusion coefficient which means that a polymer fragment diffuses farther into the warm upper surface of the film than it diffuses down toward the colder side. That this behavior was not observed in previous experiments is due to the much higher glass-transition temperatures of polymers previously used in SIMS experiments (PMMA, PS, PVP).

## Appendix B. Determination of Interfacial Phase Behavior

In this appendix, we describe the adsorption behavior of the block copolymer near the binodal phase boundary. It is seen in Figure 11a that the adsorption isotherm, calculated by SCFT, turns up sharply in the vicinity of $\phi_{AB/A} = 0.083$ and ascends vertically with small oscillations. Accordingly, there is a range of block copolymer concentrations, $0.071 \leq \phi_{AB/A} \leq 0.083$, where Γ is not uniquely defined for a given $\phi_{AB/A}$. We are not concerned with concentrations $\phi_{AB/A} > 0.083$ because this value is the location of the binodal. If attempts are made to load the film with block copolymer volume fractions in excess of 0.083, Flory−Huggins theory predicts the formation of a third block copolymer-rich phase in which all of the excess block copolymer will reside.

In Figure 16a, we focus on the portion of the adsorption isotherm in the vicinity of the binodal. Extrema in the Γ vs $\phi_{AB/A}$ plot are denoted by B through F while A denotes the origin ($\phi_{AB/A} = 0$) in Figure 11, which is off the left edge of Figure 16a. The vertical dashed line gives the location of the binodal. The region from A to B (Γ = 0−23 nm) corresponds to a monolayer, C to D (Γ = 39−55 nm) corresponds to a trilayer, and E to F (Γ = 71−88 nm) corresponds to a pentalayer. An odd number of layers is necessary to ensure that an A block

protrudes into the A homopolymer and a B block into the B homopolymer. Regions from B to C and D to E are unstable since $d\Gamma_{AB}/d\mu_{AB} > 0$ is a necessary condition for stability. It is important to note that the predicted interfacial multilayers are obtained by a one-dimensional SCFT calculation, whereas our system is three-dimensional. Our SCFT calculations contain the constraint that the amount of diblock copolymer adsorbed per unit area is constant along the plane of the interface. This constraint allows the calculation of unstable and metastable regions of the adsorption isotherm.

Determination of the value of $\Gamma$ in the $0.071 \leq \phi_{AB/A} \leq 0.083$ region requires a calculation of the free energies of the different possible interfacial phases. The appropriate free energy for comparing these different scenarios is, in fact, the interfacial energy, $\gamma$ (i.e., this is the free energy that is minimized at a set chemical potential and temperature). Results from SCFT are shown in Figure 16b where we plot the interfacial energy, $\gamma$, as a function of $\phi_{AB/A}$, over the same region as in Figure 16a. Points A through F in Figure 16b correspond to those in Figure 16a as does the vertical dashed line representing the binodal diblock copolymer concentration. Note that $\gamma$ decreases when both $\Gamma$ and $\phi_{AB/A}$ increase (A to B, C to D, and E to F), whereas $\gamma$ increases when $\Gamma$ increases but $\phi_{AB/A}$ decreases (B to C and D to E). We find from Figure 16b that the $\gamma$ values of the monolayer (A to B) are lower than those of the trilayer (C to D) and the pentalayer (E to F) at all diblock copolymer concentrations less than or equal to the binodal ($\phi_{AB/A} \leq 0.083$). Thus, a monolayer is the stable interfacial phase for all physical diblock copolymer concentrations ($0 < \phi_{AB/A} \leq 0.083$).

## References and Notes


(1) Chuai, C. Z.; Li, S.; Almdal, K.; Alstrup, J.; Lyngaae-Jorgensen, J. *J. Polym. Sci., Part B: Polym. Phys.* **2004**, *42*, 898.
(2) Xu, Z.; Jandt, K. D.; Kramer, E. J.; Edgecombe, B. D.; Frechet, J. M. J. *J. Polym. Sci., Part B: Polym. Phys.* **1995**, *33*, 2351.
(3) Adadeji, A.; Jamieson, A. M.; Hudson, S. D. *Macromol. Chem. Phys.* **1996**, *197*, 2521.
(4) Xu, G. X.; Lin, S. G. *Polymer* **1996**, *37*, 421.
(5) Washiyama, J.; Creton, C.; Kramer, E. J.; Xiao, F.; Hui, C. Y. *Macromolecules* **1993**, *26*, 6011.
(6) Bucknall, D. G.; Higgins, J. S.; Rostami, S. *Polymer* **1992**, *33*, 4419.
(7) Marti, S.; Riess, G. *Makromol. Chem., Macromol. Chem. Phys.* **1978**, *179*, 2569.
(8) Leibler, L. *Physica A* **1991**, *172*, 258.
(9) Creton, C.; Kramer, E. J.; Hui, C. Y.; Brown, H. R. *Macromolecules* **1992**, *25*, 3075.
(10) Bates, F. S.; Maurer, W. W.; Lipic, P. M.; Hillmyer, M. A.; Almdal, K.; Mortensen, K.; Fredrickson, G. H.; Lodge, T. P. *Phys. Rev. Lett.* **1997**, *79*, 849.
(11) Janert, P. K.; Schick, M. *Macromolecules* **1997**, *30*, 3916.
(12) Janert, P. K.; Schick, M. *Macromolecules* **1997**, *30*, 137.
(13) Lee, J. H.; Jeon, H. S.; Balsara, N. P.; Newstein, M. C. *J. Chem. Phys.* **1998**, *108*, 5173.
(14) Hillmyer, M. A.; Maurer, W. W.; Lodge, T. P.; Bates, F. S.; Almdal, K. *J. Phys. Chem. B* **1999**, *103*, 4814.
(15) Matsen, M. W. *J. Chem. Phys.* **1999**, *110*, 4658.
(16) Thompson, R. B.; Matsen, M. W. *Phys. Rev. Lett.* **2000**, *85*, 670.
(17) Corvazier, L.; Messe, L.; Salou, C. L. O.; Young, R. N.; Fairclough, J. P. A.; Ryan, A. J. *J. Mater. Chem.* **2001**, *11*, 2864.
(18) Morkved, T. L.; Stepanek, P.; Krishnan, K.; Bates, F. S.; Lodge, T. P. *J. Chem. Phys.* **2001**, *114*, 7247.
(19) Wang, Z. G.; Safran, S. A. *J. Phys. (Paris)* **1990**, *51*, 185.
(20) Nose, T.; Inomata, K.; Morita, H.; Kawakatsu, T.; Doi, M. *Macromol. Chem. Phys.* **2001**, *202*, 1548.
(21) Retsos, H.; Margiolaki, I.; Messaritaki, A.; Anastasiadis, S. H. *Macromolecules* **2001**, *34*, 5295.
(22) Anastasiadis, S. H.; Gancarz, I.; Koberstein, J. T. *Macromolecules* **1988**, *21*, 2980.
(23) Anastasiadis, S. H.; Gancarz, I.; Koberstein, J. T. *Macromolecules* **1989**, *22*, 1449.
(24) Shull, K. R.; Kellock, A. J.; Deline, V. R.; Macdonald, S. A. *J. Chem. Phys.* **1992**, *97*, 2095.
(25) Dai, K. H.; Norton, L. J.; Kramer, E. J. *Macromolecules* **1994**, *27*, 1949.
(26) Dai, K. H.; Kramer, E. J. *J. Polym. Sci., Part B: Polym. Phys.* **1994**, *32*, 1943.
(27) Green, P. F.; Russell, T. P. *Macromolecules* **1991**, *24*, 2931.
(28) Brown, H. R.; Char, K.; Deline, V. R.; Green, P. F. *Macromolecules* **1993**, *26*, 4155.
(29) Deline, V. R.; Brown, H. R.; Char, K. *J. Vac. Sci. Technol. A* **1991**, *9*, 1283.
(30) Bucknall, D. G.; Higgins, J. S.; Penfold, J. *Physica B* **1992**, *180*, 468.
(31) Schnell, R.; Stamm, M.; Rauch, F. *Macromol. Chem. Phys.* **1999**, *200*, 1806.
(32) Russell, T. P.; Menelle, A.; Hamilton, W. A.; Smith, G. S.; Satija, S. K.; Majkrzak, C. F. *Macromolecules* **1991**, *24*, 5721.
(33) Russell, T. P.; Anastasiadis, S. H.; Menelle, A.; Felcher, G. P.; Satija, S. K. *Macromolecules* **1991**, *24*, 1575.
(34) Genzer, J.; Composto, R. J. *Polymer* **1999**, *40*, 4223.
(35) Schnell, R.; Stamm, M. *Physica B* **1997**, *234*, 247.
(36) Fischel, L. B.; Theodorou, D. N. *J. Chem. Soc., Faraday Trans.* **1995**, *91*, 2381.
(37) Shull, K. R.; Kramer, E. J.; Hadziioannou, G.; Tang, W. *Macromolecules* **1990**, *23*, 4780.
(38) Shull, K. R.; Kramer, E. J. *Macromolecules* **1990**, *23*, 4769.
(39) Dai, K. H.; Kramer, E. J. *Polymer* **1994**, *35*, 157.
(40) Russell, T. P. *Physica B* **1996**, *221*, 267.
(41) Schwarz, S. A.; Wilkens, B. J.; Pudensi, M. A. A.; Rafailovich, M. H.; Sokolov, J.; Zhao, X.; Zhao, W.; Zheng, X.; Russell, T. P.; Jones, R. A. L. *Mol. Phys.* **1992**, *76*, 937.
(42) Schweizer, K. S.; Curro, J. G. *Phys. Rev. Lett.* **1988**, *60*, 809.
(43) Freed, K. F.; Bawendi, M. G. *J. Phys. Chem.* **1989**, *93*, 2194.
(44) Lipson, J. E. G. *J. Chem. Phys.* **1992**, *96*, 1418.
(45) Reynolds, B. J.; Ruegg, M. L.; Balsara, N. P.; Radke, C. J. *Macromolecules* **2004**, *37*, 7401.
(46) Reynolds, B. J. Ph.D. Thesis, 2005.
(47) Ruegg, M. L.; Newstein, M. C.; Balsara, N. P.; Reynolds, B. J. *Macromolecules* **2004**, *37*, 1960.
(48) Scheffold, F.; Eiser, E.; Budkowski, A.; Steiner, U.; Klein, J.; Fetters, L. J. *J. Chem. Phys.* **1996**, *104*, 8786.
(49) Matsen, M. W. *J. Phys.: Condens. Matter* **2002**, *14*, R21.
(50) Evers, O. A.; Scheutjens, J. M. H. M.; Fleer, G. J. *Macromolecules* **1990**, *23*, 5221.
(51) Helfand, E. *J. Chem. Phys.* **1975**, *62*, 999.
(52) We use $\Delta s = 20$ and $\Delta r = 4.64$ as defined in ref 45.
(53) Graessley, W. W.; Krishnamoorti, R.; Balsara, N. P.; Fetters, L. J.; Lohse, D. J.; Schulz, D. N.; Sissano, J. A. *Macromolecules* **1994**, *27*, 2574.
(54) Wignall, G. D.; Bates, F. S. *Makromol. Chem., Macromol. Symp.* **1988**, *15*, 105.
(55) Sferrazza, M.; Xiao, C.; Jones, R. A. L.; Penfold, J. *Philos. Mag. Lett.* **2000**, *80*, 561.
(56) Braslau, A.; Pershan, P. S.; Swislow, G.; Ocko, B. M.; Alsnielsen, J. *Phys. Rev. A* **1988**, *38*, 2457.
(57) Wilson, R. G.; Stevie, F. A.; Magee, C. W. *Secondary Ion Mass Spectrometry*; Wiley-Interscience: New York, 1989.


MA047539S